

Ab-initio Calculations of Energies and Self-Diffusion on Flat and Stepped Surfaces of Al and their Implications on Crystal Growth

Roland Stumpf* and Matthias Scheffler
*Fritz-Haber-Institut der Max-Planck-Gesellschaft,
 Faradayweg 4-6, D-14195 Berlin-Dahlem, Germany*
 (October 28, 2018)

Using density-functional theory we investigate several properties of Al(111), Al(100), Al(110), and stepped Al(111) surfaces. We report results of formation energies of surfaces, steps, adatoms, and vacancies. For the adsorption and diffusion of Al on flat regions of Al(111) surfaces we find the hcp site energetically slightly preferred over the fcc site. The energy barrier for self-diffusion on Al(111) is very low (0.04 eV). Coming close to one of the two sorts of close packed, monoatomic steps on Al(111), labeled according to their {111} and {100} micro-facets, Al adatoms experience an attraction of $\lesssim 0.1$ eV already before direct contact with the edge of the step. This attraction has a range of several atomic spacings and is of electronic origin. Upon arrival at the lower step edge, the adatom attaches with no barrier at a low energy five-fold coordinated site. Coming from the upper terrace, it incorporates into the step by an atomic exchange process, which has a barrier below 0.1 eV for both sorts of close packed steps. The barrier for diffusion along the lower edge is 0.32 eV at the {100}-faceted step and 0.39 eV at the {111}-faceted step. Unexpectedly the latter diffusion process proceeds by an exchange mechanism. Diffusion by a very similar exchange mechanism is also found for the “easy” direction on the Al(110) surface, i.e., along the channels. We show that Al(110) is a model system for diffusion at the {111}-faceted step on Al(111) because of its very similar local geometry. Our results enable the estimate of temperature ranges for different modes of homoepitaxial growth on Al(111). Of particular importance for the growth modes and the resulting surface morphology are the rather low barriers for diffusion across the descending steps and the rather high barriers for diffusion along the steps. We discuss the shapes of islands on Al(111) during growth and in thermodynamic equilibrium. During growth (depending on the temperature) the shape can be fractal, triangular, or hexagonal and mainly determined by kinetics; in thermodynamic equilibrium the island shape is hexagonal and determined by the different step formation energies. Many of the phenomena, which we predict for Al, were found for other metals in experiment.

I. INTRODUCTION

Atomic scale imaging techniques have proven to be useful tools to improve the understanding of atomic processes at surfaces. Prominent examples for studies at metals are the field ion microscopy (FIM) studies of self diffusion at transition metal surfaces^{1–5}, the electron microscope studies of step structures and growth on halide, semiconductor, and metal surfaces^{6,7}, and the scanning tunneling microscopy (STM) studies of the epitaxial growth and sputter removal of Pt(111).^{8–10} Several observations made in those studies like the reentrant layer-by-layer growth at low temperatures or the temperature variation of the growth form of islands at higher temperatures are not fully understood yet. For other growth phenomena like the fractal island shape at low temperatures^{9,11} a satisfying explanation does exist. Understanding the origins for different forms of growth bears technological relevance. Typically it is desirable to have layer-by-layer growth in order to produce high quality films and to achieve this at not too high temperatures.^{13–15}

How a surface develops during growth is a consequence of the microscopic adatom-surface interaction, especially at binding sites and at transition states of surface diffusion.^{16,17} If the rates for all relevant diffusion processes are known, the evolution of the surface during growth can be calculated.^{18–21} Because of the computational effort required for a quantum-mechanical description of the microscopic interaction, several quasi-classical methods have been used in the past.^{22–26} However the reliability of these calculations have always been questionable, especially because neither the influence of the kinetic energy operator for the electrons nor self-consistent rearrangements of the electron density were taken into account properly. The kinetic energy of the electrons largely determines the nature of the chemical bond by splitting the electronic energies into bonding and antibonding levels, or by influencing the charge distribution at metal surfaces, which is governed by the spill out of density into the vacuum and by the reduction of the charge density corrugation (Smoluchowski smoothing^{27,28}). All quantum-mechanical effects which are considered to be relevant for

chemisorption are taken into account in density-functional theory (DFT) to a high level of accuracy when used together with the local-density approximation (LDA) of the exchange-correlation functional.²⁹

In this paper we report a rather extensive set of DFT-LDA calculations of adsorption and diffusion of Al adatoms on different surfaces of fcc aluminum.³⁰ We even include comprehensively the diffusion at steps in our study of Al(111). The role of steps in determining the growth morphology is known since long time.⁶ We chose Al because it is a prototype of a simple *s-p* metal, hoping that the interpretation of any observation would be particularly clear and provides insights which are transferable to other systems.

Besides the flat (111), (100), and (110) surfaces, also the two different close-packed steps on Al(111) are considered. These steps are called $\langle 110 \rangle / \{100\}$ and $\langle 110 \rangle / \{111\}$ according to the step's orientation, which is the $\langle 110 \rangle$ direction, and the steepest micro-facet at their edges (see Fig. 1).^{31,32} The influence of steps is of paramount importance for the description of growth processes.^{9,21,6,33} In particular we like to understand the experimentally established differences between these two sorts of steps on (111) surfaces of fcc metals. Their slightly different geometry leads to different formation energies,⁹ to different diffusion mechanisms and energy barriers,^{10,12,34} and they are found to have different dipole moments.³⁵

Using the calculated diffusion barriers and estimated diffusion prefactors we estimated the temperature ranges for different growth modes on Al(111). To get a detailed description of the temperature dependence of the growth of the Al(111) surface one should use our results on surface diffusion as input for a theory^{18–21} which solves for the rate equations which determine the evolving surface morphology during growth. This still remains to be done.

The paper is organized as follows. First we give a short description of our *ab-initio* method and describe some technical aspects which make it particularly efficient for the calculation of large metallic systems. Section III describes differences in the formation energy of the two sorts of close-packed steps on Al(111). In Section IV we discuss the adatom- and step-induced dipole moment on Al(111) and, connected to that, the work function differences between Al(111), Al(100), and Al(110). In Section V the surface self-diffusion is investigated, first on the flat Al(111) surface, then approaching a step, and finally at the step. Also vacancy diffusion on the flat Al(111) surface is considered. We compare the self-diffusion on Al(110) with that on the stepped Al(111) surface and we compare diffusion at the two different steps on Al(111). In Section VI we describe some uniformity in surface self-diffusion on fcc metals, which help us to estimate diffusion prefactors for the self-diffusion on Al surfaces. Using the calculated diffusion barriers and the estimated prefactors, we summarize in Section VII our understanding of the temperature dependence of atomic transport processes and of homoepitaxial growth on Al(111). In the appendix we also present some results for the self-diffusion on Al(100).

II. THEORY

The computer code, **fhi93cp**, used in this study is described in Ref. 36. We therefore summarize here only some essentials of the method. We use density-functional theory and treat the exchange-correlation functional in the local-density approximation.³⁷ The Kohn-Sham equations³⁸ are solved by a Car-Parrinello-like iterative scheme³⁹ using the steepest descent approach⁴⁰ for the update of the wavefunctions. We use a fully separable *ab-initio* pseudopotential⁴¹ for Al where the *d*-potential is treated as local and *s* and *p* potentials are described by projection operators. The electronic wavefunctions are expanded in a plane-wave basis set with a kinetic energy cut-off of 8 Ry. The Brillouin zone is sampled at special \mathbf{k} -points,⁴² which are specified below for the different systems when these are discussed.

In the following we describe in more detail the *damped Newton dynamics* procedure to relax atoms, the Fermi surface smoothing technique, and some technical improvements, which allow us to calculate large systems. We also describe the geometry of the systems investigated and estimate the numerical accuracy of our results.

A. Atomic relaxations

In our adsorption calculations we typically allow the Al adsorbate and the top two (111) layers or three (110) layers to relax until all force components are smaller in magnitude than 0.04 eV/Å. It was checked that relaxation of an additional layer leaves the adsorption-energy differences practically unchanged. The most important effect of the adsorbate-induced substrate relaxation is a reduction of barriers for bridge diffusion by 0.07 ± 0.05 eV.

The algorithm to relax the atomic geometry is based on *damped Newton dynamics*. In a finite-difference form the time evolution of any atomic coordinate X is given by

$$X^{\tau+1} = X^{\tau} + \eta_X (X^{\tau} - X^{\tau-1}) + \delta_X F_X^{\tau}, \quad (1)$$

where X^τ is the coordinate at time step τ and F_X^τ the force on X at time step τ . The parameters η_X and δ_X control the damping and the mass of the coordinate. The choice of those parameters is guided by the goal that this classical dynamics combines a fast movement of the atoms towards the next local minimum of the Born-Oppenheimer surface and avoids oscillations around it. We got fast convergence for our Al surface systems with $\eta_X \approx 0.6$ and $\delta_X \approx 8$. This choice brings the calculations close to the aperiodic limit of a damped oscillator in classical mechanics. Increasing the damping coefficient η_X improves the stability of the atomic relaxation process, reducing it allows for energy barriers to be overcome and so to escape from local minima. In it's usage of the knowledge of the history of displacements the damped dynamics technique is similar to the conjugate-gradient technique.⁴³

Obviously the atomic geometry converges faster when larger displacements per time step are executed. The magnitude of useful displacements is restricted, however, by the efficiency with which the electronic wavefunctions converge to the electronic ground state of the new atomic coordinates after the displacement. We found it advantageous to have about eight purely electronic iterations after any atomic displacement. Note that the time-consuming calculation of the atomic forces is not done in those purely electronic iterations. For all systems studied in this paper about ten atomic relaxations are necessary to converge to the desired accuracy.

B. Fermi occupation

In order to stabilize the self-consistent calculations for the electrons and to improve \mathbf{k} -space integration, we smear out the Fermi surface. For this purpose the Kohn-Sham eigenstates of energy ϵ_i are occupied according to a Fermi distribution $f = f(\epsilon_i, T^{\text{el}})$ with $k_B T^{\text{el}} = 0.1 \text{ eV}$. Using the Fermi distribution implies that the free energy $F = E - T^{\text{el}} S$ at the electronic temperature T^{el} is minimized instead of the total energy E .⁴³⁻⁴⁶ Here S is the entropy of independent electrons,⁴⁷

$$S = -2k_B \sum_i [f_i \ln f_i + (1 - f_i) \ln(1 - f_i)] . \quad (2)$$

This approach may cause some inaccuracies, as we want to get results belonging to $T^{\text{el}} = 0$. For the free energy at a given geometry the $T^{\text{el}} \rightarrow 0$ limit can be easily obtained by evaluation of $E^{\text{zero}} = 0.5(E + F) = E - 0.5T^{\text{el}} S$.⁴³⁻⁴⁵ This value differs from $F(T^{\text{el}} \rightarrow 0)$ only by terms which are third and higher order in T^{el} . For the optimization of the geometry the force $\partial E^{\text{zero}} / \partial X$ should be used which is, however, more complicated to evaluate.⁴⁸ For our choice of $k_B T^{\text{el}} = 0.1 \text{ eV}$ the geometries and the total-energy differences are almost not affected. This was tested for the adsorption of Al on Al surfaces by using values of 0.05 eV and 0.2 eV for $k_B T^{\text{el}}$ and an increased number of \mathbf{k} -points.

A further approach to stabilize the way self-consistency is achieved is to reduce electron transfer between single-particle states in successive iterations. For this purpose fictitious eigenvalues after Pederson and Jackson⁴⁹ are introduced. The occupation numbers are calculated directly from the fictitious eigenvalues according to Fermi occupation at T^{el} . These fictitious eigenvalues follow the as-calculated eigenvalues in a sort of damped dynamics, so that both sets of eigenvalues will become identical when self-consistency is attained. This indirect approach of damping charge transfer oscillations is easier to implement than the more obvious one of damping the change in occupation numbers directly. The reason is that the occupation numbers are constrained to be in the range between 0 and 2, and their sum has to give the total number of electrons. For the eigenvalues no such constraints exist.

C. Optimizations

The computer code is optimized for large systems by using the following concepts. Because the evaluation of the non-local part of the pseudopotential dominates the computation time for large systems we utilize the translational symmetry for those atoms sitting on ideal lattice sites.³⁶ Without introducing any approximation this optimization typically reduces the number of operations by a factor of ten for these atoms.

One often encountered problem with large systems is the $1/G^2$ dependence of the electrostatic potential. Here \mathbf{G} is a reciprocal-lattice vector. This dependence leads to long-wavelength charge-density oscillations, known as *charge sloshing* or *$1/G^2$ instability*. See for example Ref. 50. We deal with this problem by starting with a rather good initial density constructed by a superposition of contracted atomic charge densities. The contraction was done following Finnis,⁵¹ where the radial atomic densities are multiplied by a Fermi function. The contraction anticipates most of the intra-atomic charge transfer that occurs upon building a solid from isolated atoms. The wavefunctions for the first step of the self-consistent iterations are obtained by diagonalizing of the Kohn-Sham Hamiltonian constructed from this approximate density and within a reduced plane-wave basis ($E^{\text{cut}} = 1.5 - 5 \text{ Ry}$, depending on time and memory

constraints). Then, in the first $\hat{\tau} < 8$ electronic iterations, the charge density $n(\mathbf{r})$ is linearly mixed like in “standard” self-consistent calculations:

$$n^{\text{in},\hat{\tau}+1}(\mathbf{r}) = \alpha n^{\text{out},\hat{\tau}}(\mathbf{r}) + (1 - \alpha)n^{\text{in},\hat{\tau}}(\mathbf{r}) . \quad (3)$$

We use a mixing coefficient α which increases from 10% to 100% within these first eight time steps. By this procedure the charge sloshing was not initiated for the systems considered in this paper and so did not cause problems during the rest of the calculations. In calculations of larger cells than those reported here we found the linear mixing in \mathbf{r} -space insufficient. The charge density sloshing could however be efficiently suppressed by a mixing in \mathbf{G} -space with a mixing coefficient $\alpha(G)$ which was chosen smaller for smaller G .

For large systems the required computer memory raises as the square of the number of atoms and it is largely determined by the number of wavefunction coefficients. We optimize memory usage in several ways. A simple steepest-descent update procedure for the wavefunctions is used⁵² so that only the wavefunction coefficients of one iteration need to be stored. The wavefunction coefficients and most of the other large arrays are stored in single precision; however, double precision is used for all floating point operations and for storing intermediate results.

Our computer code optimizes the data access in computers which use memory of different speed. The idea is that once data is transferred from slow memory to fast memory, e.g. from the disk to main memory, this data should be used as often as possible before it is moved back to the disk. This improvement can be accomplished by reordering loops or by blocking techniques.³⁶ The most important case where blocking is used is the orthogonalization of the wavefunctions. Instead of orthogonalizing always one wavefunction to those with lower index (the standard Gram-Schmidt procedure), we orthogonalize a block of, say, 30 wavefunctions to those with lower index and then orthogonalize the wavefunctions within the block. In the case where only part of the wavefunctions at one \mathbf{k} -point fit into main memory this procedure reduces the disk to memory data transfer by a factor up to 30.

An example of the efficiency of the code is the calculation of an Al slab with 350 atom per unit cell in a supercell as large as 560 atomic volumes, and sampling the Brillouin-zone at one special \mathbf{k} -point. This leads to 28 000 plane waves, to 560 involved electronic states, and an overall memory requirement of 200 MB. This calculation takes about 25 h on an IBM/6000 370 RISC workstation with 64 MB main memory, if all atoms sit on ideal lattice positions. If no atoms are sitting on ideal sites, the time increases by a factor of three. The time spent waiting for disk access during the calculation is below 30% and could even be reduced noticeably by using the faster hard disks available today.

D. Slab geometry

In order to describe an adatom on a crystal surface we use a slab in a supercell. The repeating slabs are isolated by $\gtrsim 8\text{\AA}$ of vacuum spacing. For the purpose of studying practically isolated adsorbates, the distance between adatoms in neighboring cells is at least three nearest-neighbor spacings. This results in an interaction energy below 0.03 eV for Al adatoms.

In order to have more bulk like layers and to avoid artificial adsorbate-adsorbate interaction through the slab, we adsorb the Al adatom only on one side. This approach reduces the slab thickness necessary for the desired degree of accuracy.⁴⁴ Due to the unsymmetrical situation an artificial electric field perpendicular to the slab might arise. This field is compensated in our calculations as described in Ref. 44, by introducing a dipole layer in the vacuum region. In the case of an Al adsorbate on an Al surface this field is always very small so that even in the uncompensated case the energy differences between different sites are practically unaffected.

For the calculation of adsorption on Al(111) we use typically normally 5-layers-slabs. Calculations with slabs of 4, 6, and 7 layers show that even with a 4 layer slab adsorption energy *differences* are accurately given, which means that they change by less than 0.03 eV when thicker slabs are used.

For Al(100) we find that the desired accuracy of 0.03 eV requires a slab thickness of at least 6 layers. The quantity most sensitive to the slab thickness is the energy barrier for exchange diffusion; for a 5 layer slab this is by 0.25 eV or 66% lower than that of the 6- and 7-layers thick slabs (see Appendix A). We use a 4×4 surface cell for the calculations of self-diffusion on Al(100). For the Al(110) surface we used 8 layers and a 3×4 surface cell.

In this paper we treat the two densely packed steps on Al(111). One is called {111}-faceted, the other {100}-faceted (see Fig. 1). The {111} and {100} micro-facets are the steepest ones and therefore give an unambiguous way of naming the steps.³¹ We shall see, however, that the electronic properties of the {111}-faceted step are more closely related to the (110)-surface. This similarity was already discovered by Nelson and Feibelman,⁵³ who showed that the relaxation of the Al(110) surface atoms and the atoms close to the (110)/{111} step is very similar and that the charge densities at the Al(110) surface and along the {110} plane through a (110)/{111} step are nearly identical. Our calculations confirm this and also show the similarity of chemical properties and of self-diffusion on the Al(110) surface and at the {111}-faceted step.

In order to analyze the step properties we use three different approaches. In the first approach a slab in (111) orientation is put in an orthorhombic supercell. Then half of the atoms of the top layer are removed, so that the remaining grooved surface has two steps, one being {111}- and the other {100}-faceted (see Fig. 1; the lower part of the supercell, containing the flat termination of the slab and some more vacuum, is omitted in the upper panel of Fig. 1). We choose different sizes of the surface supercell to study the influence of finite size effects. The width of the cell in [110] direction is varied from three to four atoms and the width of the terrace in [112] direction is three to four atomic rows. All these systems give results which differ only by ≤ 0.05 eV. One reason for this is the rapid screening of Al. The other reason is that quantum size-effects are often unimportant for total-energy differences on stepped Al(111) which was already noted by Nelson and Feibelman.^{53,54}

The second approach uses a class of systems which are slabs of $(m, m, m-2)$ and of $(m+2, m, m)$ orientation where m is an even number. Surfaces with these Miller indices are vicinal to the (111) surface. The $(m, m, m-2)$ surface consist of terraces of (111) orientation which are m atomic rows wide and separated by {111}-faceted steps. The $(m+2, m, m)$ surface has (111) terraces $m+1$ atomic rows wide, which are separated by {100}-faceted steps.³¹ The relationship between the Miller indices of the vicinal surfaces and the constituent low index facets can be seen by the vector decompositions $(m, m, m-2) = (m-1) \times (111) + 1 \times (11\bar{1})$ and $(m+2, m, m) = m \times (111) + 1 \times (200)$. Note that conventionally common factors are removed from Miller indices, so that instead of (200) [which is the shortest reciprocal lattice vector in the (100) direction] the more familiar (100) is used and for even m the common factor two is removed. Thus the Miller indices are $1/2 \times (m, m, m-2)$ and $1/2 \times (m+2, m, m)$.

We worked with surfaces belonging to even m because they can be accommodated in a monoclinic supercell, whereas for odd m a triclinic supercell is required. The first surface (i. e. $m = 2$) of the $(m, m, m-2)$ family is the $(220)\equiv(110)$ surface, for which the (111) terraces are so narrow that no surface atom has a (111)-like coordination. After some test calculations with the (221) surface ($m = 4$), we concentrated on the (332) surface ($m = 6$) for studying the properties of nearly isolated {111}-faceted steps. The (332) surface has (111) terraces which are six atomic rows wide (see Fig. 2). We used a 1×4 surface unit cell, which means that 6×4 atoms are exposed at the surface. This layer is repeated six times to build a slab containing 144 atoms per cell.

For studying the properties of nearly isolated {100}-faceted steps we used the (433) surface out of the $(m+2, m, m)$ family, which contains seven atomic rows of (111)-orientation. With a 1×4 surface unit cell, we get 7×4 atoms exposed on each surface (see Fig. 3). Again, 6 layers were taken which gives a slab containing 168 atoms per cell.

The adsorption calculations at the steps of the (221), (332), and (433) surfaces essentially reproduce the results of the grooved surfaces, which reflects the efficient screening at Al surfaces. This agreement of results obtained for different slabs also provides a good test of the convergence of our calculations with respect to system size and \mathbf{k} -space sampling.

The main advantage of using the vicinal surface systems is that they allow the investigation of long-range adsorbate-step interactions, which were found for example experimentally by Wang and Ehrlich,⁵⁵ for a given adsorbate-step distance the number of atoms in the cell is only slightly more than half of that required for the grooved slab geometry.

For the purpose of calculating the difference in step formation energy of {111}- and {100}-faceted steps a third kind of system has to be used. It should contain only one kind of step and it should provide a favorable error cancellation when the energy *difference* of the {111}- and {100}-step systems is determined. The chosen system consists of a triangular Al island on Al(111) with either {111}- or {100}-faceted edges, depending on the triangle's orientation. Note that this way the number of atoms and the \mathbf{k} -space integration is the same for both step orientations. One new uncertainty in determining the step formation energy difference is now introduced however: also the corners of the triangles contribute to the difference. The contribution of the corners has to be removed by extrapolating to the thermodynamic limit of infinite island size. The largest triangles studied consisted of 21 atoms in a 8×7 Al(111) surface cell. At a slab thickness of 4 layers this gives 245 atoms per supercell.

E. Estimated accuracy

The equilibrium lattice constant for a basis set with 8 Ry cut-off and a \mathbf{k} -point sampling like that used for the surface calculations is 3.98 Å (including zero-point vibrations),⁴⁴ which is 0.7% smaller than the experimental value. The cohesive energy is 4.15 eV, which is 0.75 eV higher than the experimental one of 3.40 eV.⁵⁶ These errors in bulk results are within the expectations for a well-converged DFT-LDA calculation.

The 8 Ry plane wave cut-off was tested to be sufficient to converge adsorption energy *differences* to a numerical accuracy better than 0.02 eV (see also Ref. 44). Because of the large size of our supercells – they comprise, depending on the problem, 140–560 atomic volumes – one special \mathbf{k} -point⁴² in the irreducible quarter of the surface Brillouin zone, which is always nearly square, is sufficient to give energy differences which are within 0.03 eV of those obtained by using two or four times the number of \mathbf{k} -points.

We also tested the dependence of our results on system size. Here the slab thickness as well as the adsorbate-adsorbate and the step-step interactions are relevant. System size and \mathbf{k} -space-sampling effects are difficult to separate, because often a change of the size of the system implies different \mathbf{k} -sampling, and the two effects are about equal in magnitude. We therefore cannot quantify the error introduced by system size effects separately. In order to reduce errors from these two sources we always quote the mean value of calculations at different \mathbf{k} -point sampling and system size. This improves the accuracy because the variations with system size and \mathbf{k} -space sampling are often oscillatory. We obtain an overall numerical accuracy of the energy differences given of ≤ 0.06 eV, unless a different error margin is stated explicitly.

III. DIFFERENCES OF IDEAL {111} AND {100} FACETED STEPS

Calculations of the average energy of the two step types can be performed most accurately by investigating the total energy of surfaces with terrace stripes (see Fig. 1), and comparing these results to those of the flat surface. The mean step formation energy is determined as 0.24 eV per step atom. Table I shows that this is about half of the energy required to create the Al(111) surface per surface atom, and that the step formation energy compares to the difference of the surface energies between Al(111) and the rougher (100) or (110) surfaces per atom.

The energy difference of the two step types can be obtained by investigating triangular islands adsorbed on Al(111), as these contain only one type of steps (see Fig. 4). Comparing islands with 6, 10, 15, and 21 atoms we can extrapolate to the limit where the influence of the corner atoms is negligible. Table II lists the results for the total-energy differences of two triangles whose orientations differ by 60° , and hence have different step types. The data show the rapid convergence of this energy difference with island size. Dividing these energy differences into an island size independent contribution from the three corner atoms and a contribution proportional to the number of true edge atoms a fit to our data (see Table II) gives the following results. Triangular islands with {111}-faceted steps are more favorable by 0.025 eV per corner and by 0.017 eV per true step atom than islands bounded by {100}-faceted steps. The energy differences are almost the same, whether the island atoms are relaxed or not. This small effect of relaxation shows that the step formation energy difference is an electronic effect and is not determined by a different step-induced atomic relaxation. It is interesting that our results cannot be estimated from simple embedded atom or effective medium theory^{24,25,57} or a bond-cutting model.⁶⁰ The reason is that the two different triangular islands have exactly the same number of bonds.

From the step formation energy one can directly obtain the equilibrium shape of larger islands by minimizing the island free energy for a given number of atoms in the island. The graphical solution of this optimization problem is called the Wulff construction.²⁸ As a result one obtains hexagonally-shaped islands, where the edges alternate between those with a {100} and those with a {111} micro-facet. The calculations predict that in thermodynamic equilibrium the {111}-faceted edge should be longer with a edge length ratio $L^{(110)}/\{100\} : L^{(110)}/\{111\}$ of 4 : 5. Effects of the vibrational or the configurational entropy on the length ratio, which might be important at higher temperatures, are neglected.

It is interesting to note that such hexagonal islands have been observed experimentally by Michely and Comsa³² in their STM studies of growth and sputter removal of Pt(111). These experiments show that the {111} micro-facet is favored which is what we predict for Al(111). There is a quantitative difference, since for Pt(111) the measured edge-length ratio is 0.66, i.e. 2 : 3. The similarity to our results is much more than what one would have expected, as, in general, Al and Pt behave quite differently.

IV. WORK FUNCTION DIFFERENCES AND INDUCED SURFACE DIPOLE MOMENTS

Our calculations of induced surface dipole moments and work function differences at Al surfaces give unexpected results.

The first interesting observation is that the Al(111) surface and the Al(110) surface have about the same work function Φ . Our best converged results are $\Phi_{\text{Al}(111)} = \Phi_{\text{Al}(110)} = 4.25$ eV,⁶³ the experiment finds $\Phi_{\text{Al}(111)}^{\text{exp}} = 4.24$ eV and $\Phi_{\text{Al}(110)}^{\text{exp}} = 4.28$ eV.⁶²

The second result is that steps on Al(111) do not affect the work function very much. Table III lists the induced dipole moment μ per step atom. The {111}-faceted step induces practically no dipole ($\mu = -0.01$ debye), the {100}-faceted step has a small dipole moment with the negative end pointing into the vacuum ($\mu = 0.045$ debye), which means that they increase the work function. Induced dipole moments translate into work function changes $\Delta\Phi$ according to the Helmholtz equation

$$\Delta\Phi = 135 \cdot \frac{\mu}{A} \quad (4)$$

with μ in debye, $\Delta\Phi$ in eV, and the area A per dipole in bohr².

More noticeable dipole moments are found for 3-fold coordinated Al adatoms (see Table III). An example is the dipole moment of 0.24 debye for an Al adatom on the hcp-site. If there was an adlayer of those Al adatoms on Al(111) of, say, 1/10 monolayer coverage, the work function would increase by 0.13 eV.

The reported results on induced dipole moments and work function differences contradict the traditional model of charge redistribution at rough metal surfaces and around protrusions on metal surfaces like steps or adatoms.^{64,28} This model is based on Smoluchowski smoothing. Smoluchowski smoothing is driven by the kinetic energy of the electrons which is lower for a less corrugated charge density. The smoothing of the charge density lowers the work function for rougher surfaces and causes a induced dipole moment with the positive end towards the vacuum for protrusions on the surface. The smoothing effect is often discussed in a nearly free electron picture. An example is the calculation by Ishida and Liebsch⁶⁵ of the induced dipole moment of steps on jellium. They find that steps reduce the work function. Extrapolating their results for a step on Al(111) one gets an induced dipole moment of about -0.07 debye per step atom equivalent.

The reason why the smoothing model fails in our calculation of atomic Al could be that the smoothing effect, which is certainly there, is (over-) compensated by the attraction of electrons towards the deeper potential around surface atoms on Al(110), step-edge atoms on Al(111), or adatoms on Al(111). These atoms are only 7- or 3-fold coordinated as compared to the 9-fold coordinated surface atoms. Therefore they are less well screened, which leads to the deeper potential in their vicinity. This effects a net transfer of electrons towards those undercoordinated atoms. A more thorough discussion of the charge rearrangements in different surface geometries and the resulting induced dipole moments will be published elsewhere.⁶⁶

Having a possible explanation why the standard model fails in the case of the simple metal Al the remaining puzzle is why it seems to work for the transition metals.⁶⁴ To give an example. Steps on Au(111) and Pt(111) show dipole moments between -0.25 debye (Au) and -0.6 debye (Pt) per step atom.³⁵ A comparison with the jellium calculations in Ref. 65 shows that for those steps the induced dipole moment is larger in magnitude than it would be expected from the smoothing effect of the *s-p* like electrons only. The additional negative dipole moment is likely caused by a polarization of the *d*-electrons of the step atoms. This would also explain why Au shows a smaller effect than Pt. Au has a filled *d*-shell, in Pt the Fermi level cuts the *d*-band and therefore it is easier to polarize the *d*-states.

We see that for the simple as well as for the transition metals important additions to the smoothing based model for induced surface dipole moments and work function differences have to be made.

V. AL ADATOMS ON FLAT AND STEPPED AL(111)

This section describes the total-energy surface for an Al adsorbate atom on the flat Al(111) surface and at the {100}- and {111}-faceted steps. This discussion is directly relevant for surface diffusion and crystal growth on Al(111). We will study how an Al adatom moves across the Al(111) surface, what happens when the adatom comes close to a step, how it attaches to the step coming from the lower side, and how it incorporates into the step by an atomic replacement process coming from the upper side.

A. Diffusion on flat Al(111)

The diffusion energy barriers of an isolated Al adatoms on the flat Al(111) surface is very small (0.04 eV; see Table IV and Figs. 5 and 6). The hcp site is the stable binding site and the energies of bridge and fcc sites are almost degenerate. The diffusion path between the hcp sites is the direct connection between adjacent hcp, bridge, and fcc sites.

The only marked maximum of the total-energy surface is at the atop site. The top site is 0.53 eV higher in energy than the hcp site. Interesting about the atop site is the low height of the adatom at the atop site which is close to the height in the 3-fold sites (see Table IV). This is a consequence of the fact that bond length gets smaller when the coordination is lower (for the atop site we obtain a bond length of 2.51 Å which is 6 % smaller than for the 3-fold sites). Furthermore, we find that the adatom at the atop site introduces a strong substrate relaxation: the substrate atom below the adsorbate is lowered by 0.4 Å. A similar substrate relaxation was found in calculations for alkali-metal adsorbates on Al(111).^{44,67}

The height of the diffusion energy barrier of 0.04 eV is at the lower limit of an energy barrier one would expect for this close-packed surface from experimental data (see Table V). Two features of the total-energy surface are worth discussing further.

We first note that it is unexpected that the hcp site is the equilibrium site for low coverage. The hcp and fcc sites both provide threefold coordination, but only the fcc site continues the ABCABC stacking of the fcc crystal, whereas the hcp site belongs to an ABCAC stacking. A simple continuation of the fcc structure would suggest that the fcc site should be occupied. In fact, the fcc-hcp energy difference is coverage dependent. Above 1/4 ML coverage the fcc site gets more stable. To create a full monolayer of Al at the hcp position costs 0.05 eV per surface atom compared to the fcc stacking. It is interesting that this energy is exactly the mean of the formation energy of the three bulk stacking faults in the $\langle 111 \rangle$ -direction, which were calculated by Hammer et al.⁶⁸

The reason for the different adsorption energy at the hcp and fcc sites at low coverage is not obvious. Half of the difference exists already before the Al(111) substrate is relaxed, which shows that there is an electronic contribution. Another hint for an understanding might be that the Al adsorbate at the fcc site has a larger induced dipole moment than at the hcp site (see Table III).

The second interesting feature of Al on Al(111) is that the three-fold coordinated fcc sites and the two-fold coordinated bridge sites have practically the same total energy. This is not explainable in a coordination number model.⁶⁰ One might guess that the rather favorable energy of the bridge site is a result of the substrate relaxation. Indeed, on the unrelaxed substrate the bridge site is energetically less favorable (but only by 0.07 eV) than the fcc site. If the atomic geometry were not relaxed and all atoms are kept at bulk nearest neighbor spacings, then the fcc site were favored by 0.13 eV over the bridge site. Still, this is much less than what a coordination number model would predict.

The energy difference between hcp, bridge, and fcc sites is very small. It is therefore important to check, if the calculations are sufficiently accurate. We therefore performed several test calculations, varying carefully all parameters which affect the accuracy. We used coverages from 1/12 to 1/56 ML, increased the number of \mathbf{k} -points from 1 to 4 and to 9, we used from 4 to 7 Al(111) layers, and we increased the plane wave cut-off. The energy differences of different sites were very stable and the order of fcc and hcp site never reversed at low coverage. We expect the difference between hcp and fcc site to be accurate to within 0.02 eV. The relative accuracy for the bridge site is slightly worse. Feibelman's recent LDA calculations⁵⁴ found the hcp site more stable than the fcc site by 0.03 eV, in good agreement with our results.

In order to get an idea of the nucleation probability and the influence of adsorbate-adsorbate interaction on the mobility we calculated the adsorbate-adsorbate interaction between two Al adatoms sitting at neighboring hcp-sites. The energy gain with respect to isolated adatoms is 0.58 eV. We note, however, that only one configuration (hcp-hcp) was considered and we did not perform any of our usual checks, so that here an error of ± 0.2 eV might be possible.

B. Approaching the step

Table IV and Figs. 5 and 6 show that the Al adatom is attracted by the step on the lower as well as on the upper terrace and that this is similar for both sorts of steps. This attraction leads to an energy gain of about 0.1 eV at the threefold sites directly at the upper step edge compared to the flat Al(111) surface. The long-range attraction towards the step as experienced by atoms on the lower terrace is weaker, but at closer distance the attraction gets as strong that the last two threefold sites before the fivefold at-step site are not local minima any more and an adsorbate there will be funneled towards the step directly.

This attraction and the funneling of Al adsorbates by the lower step edge resembles the behavior found recently by Wang and Ehrlich for Ir on Ir(111).⁵⁵ Also on Pt(111) indications of a funneling towards steps exist.⁹ Finding the same behavior for different metals suggests that the medium-range to long-range attractive interaction is a more general phenomenon. Therefore, an understanding of the nature of the mechanism behind this attraction of adatoms towards steps is desirable. We approach the analysis of its origin by considering the following thinkable mechanisms and check whether they are indeed attractive or not. The mechanisms are dipole-dipole interaction, elastic interaction, and interaction of defect induced surface-states.

The analysis shows that the mechanism is not an attractive dipole-dipole interaction. The dipole-dipole interaction in the studied cases will be very weak. Even for the largest dipole moments (those for adatoms at the fcc site and for the {100} step, see Table III) the interaction energy would be below 1 meV for distances larger than one nearest-neighbor spacing. Furthermore we note that the interaction would be *repulsive*.

Another possible mechanism responsible for the attractive adatom-step interaction could be the elastic interaction of the adsorbate-induced and the step-induced relaxation fields. This possibility can easily be checked by a calculation of the energy while keeping the substrate atoms at their ideal positions. Our calculations show that the long-range interaction remains unchanged. Thus, elastic effects can be disregarded as the origin of the attractive interaction

between the adatom and the step. The fact that the adatom-step attraction is not of elastic origin and that it is long range excludes the possibility that it can be reproduced with more simple bonding models like coordination number models⁶⁰ or effective medium and embedded atom.^{58,59}

In consequence there remains only the possibility that the attractive interaction is caused by an interaction of adatom-induced and step-induced surface states or screening charge densities. This conclusion is supported by recent STM pictures of adsorbate and step induced surface states on Cu (111) and Au (111).^{71,72}

C. Comparison of self-diffusion on the flat Al(110) surface and at the {111}-faceted step on Al(111)

Figure 7 shows five geometries which we consider to be particularly important for diffusion on the Al(110) surface and at the {111}-faceted step on the Al(111) surface. In the following we will compare the two systems and we will analyze the factors determining the adsorption energies in different bonding geometries. The results of Table VI show that at geometries having the same nearest-neighbor environment, the adsorption energies are very similar on the (110) surface and at the {111}-faceted step.

At the two fivefold sites (Fig. 7(a)) the adsorption energy is rather large and practically identical in both cases. The calculated Al bulk cohesive energy is only 7% or 0.27 eV larger. The adsorption energy on the threefold equilibrium site on Al(111) at low coverage (the hcp site) is as much as 20% or 0.78 eV smaller (Table IV). A coordination number model⁶⁰ would give too small an estimate of the adsorption energy. The high at-step adsorption energy we understand as follows. At both fivefold sites the adsorbates sit in a valley which should be filled with additional electronic charge due to Smoluchowski-smoothing.²⁷ Additionally the adsorbates sit very close to the surface. On the (110) surface the height at the fivefold site is 1.33 Å relative to the relaxed clean surface. This should be compared to the hcp site on Al(111), where the height of the adsorbate is 2.09 Å. The combination of increased charge density and low height provides a good embedding of the adsorbate.⁵⁷

D. Adatom at bridge sites

The twofold coordinated bridge sites are possible saddle point configurations for surface self-diffusion. The energies of the comparable bridge sites on Al(110) and at the {111}-faceted step are similar. However, the two different bridges (see Figs. 7(b) and 7(c)) have a markedly different energy. This energy difference gives rise to a difference in barrier height of a factor of two (see Table VI). What is the reason for this difference of sites with the same coordination? Our explanation is the same as for the high adsorption energy at the 5-fold site. The higher adsorption energy for the long bridge is accompanied by a lower distance to the surface. For the long bridge on the (110) surface the adatom height is only 1.58 Å, whereas the height is 2.16 Å for the short bridge. Another effect should be that Smoluchowski-smoothing fills the valleys with electron density taken from the upper part of the rows on the clean surface. For the short-bridge position, this would reduce the charge density around the adsorbate, while it would rather increase the embedding charge density for the long bridge position.

Having seen the striking similarity of adsorption energies at the (110) surface and at the {111}-faceted step, it is no surprise that a system which lies between the two cases, namely the (331) surface, shows a very similar behavior.⁵⁴ For this system Feibelman obtained energy differences between the Al adsorption at 2-fold and 5-fold sites which are very close to ours (see Table VI). We expect that the agreement with our results would be within 0.05 eV if Feibelman would have included the adsorbate-induced relaxation of the substrate. The agreement of both studies is a most demanding test for the numerical accuracy of both calculations, since Feibelman used a rather different technique.

We will now show that the just discussed bridge sites are not the lowest energy transition states for diffusion for the surfaces considered. Diffusion takes place preferably via exchange mechanisms.

E. Exchange process for diffusion parallel to {110}/{111} steps on Al(111) and along the channels of Al(110)

Investigating the Al(110) surface we will first show that the exchange mechanism lowers the energy barriers for diffusion, and this holds even in the so called easy direction, i. e. for diffusion in the channels of this surface. Figure 7(d) sketches the symmetric configurations of the exchange paths. For both the (110) surface and for the {111}-faceted step, the geometry may be described as two fivefold coordinated Al adatoms which are close to a surface vacancy. At the (110) surface the two atoms are displaced from the ideal fcc lattice positions by 0.08 Å towards the vacancy and they are 0.05 Å closer to the surface than for the “normal” fivefold site. At the step the corresponding displacements are similar. To get some insight into the nature of bonding of this configuration, we estimate its energy from the adsorption energy

of the “normal” fivefold site E_{ad} and the calculated vacancy-formation energies, where the Al chemical potential, which defines the energy of the removed Al atom, is taken as the bulk cohesive energy, i. e. 4.15 eV. For the vacancy formation energy at the (110) surface we then obtain 0.12 eV and at the step the result is $E_{\text{step}}^{\text{vac}} = 0.21$ eV (see Table I). The energy barriers are then estimated as $E_{(110)}^{\text{vac}} - E_{(110)}^{\text{ad}} = 0.38$ eV and $E_{\text{step}}^{\text{vac}} - E_{\text{step}}^{\text{ad}} = 0.49$ eV, in close agreement with the full calculation of the exchange-parallel processes in Table VI.

Up to now we have only discussed the symmetric configurations of the exchange diffusion path (see Fig. 7 (d)) without knowing if these are really saddle point configurations. Additional calculations at the step show that they are *not* saddle points, but that they correspond to very shallow minima of the total-energy surface. The saddle points found in these calculations have an energy about 0.04 eV higher than the energy of the symmetric configuration. This energy difference is about 1/10 of the total energy barrier and also very small compared to the numerical accuracy of our calculations. It is therefore appropriate to discuss the energy for the symmetric exchange configuration when talking about diffusion barriers.

In addition to the discussed mechanisms a third diffusion mechanism for diffusion along the channels was recently proposed by Liu et al.²³ They argue that the configurations of Fig. 7 (e), which are saddle point configurations for the diffusion perpendicular to the channels, are also approximately saddle point configurations for the diffusion parallel to them. This would imply that the diffusion parallel and the exchange diffusion perpendicular to the rows would have about the same energy barriers. This idea is interesting, but we get a higher energy barrier for the perpendicular than for the parallel exchange process (see next paragraph and Table VI). Thus, for Al we cannot support the idea²³ but nevertheless, the proposed process could be the explanation for the near identity of parallel and perpendicular to step diffusion energy barriers on Ni, Ir, and Pt (see Table V).

F. Exchange process for diffusion perpendicular to $\langle 110 \rangle/\{111\}$ steps on Al(111) and to the channels of Al(110)

We now discuss the exchange perpendicular to the channels of Al(110) and across the $\langle 110 \rangle/\{111\}$ step on Al(111) (see Fig. 7 (e) and 5). Again the energies of the saddle point configuration on Al(110) and at the step are similar (see Table VI). The slightly higher energy of the saddle point geometry at the step can be understood in terms of the higher vacancy formation energy at the step (see Table I) and of the threefold rather than fourfold coordination of the upper Al atom. On Al(110) the energy of the exchange configuration can be estimated analogously to our discussion in the last Section. The configuration consists of two neighboring fourfold coordinated atoms close to a vacancy. We want to approximate the energy of the fourfold coordinated atoms by that of another fourfold atom adsorbed at the same height. There is however some ambiguity in assigning a height to the two adsorbates. The possibilities are to take the distance of 0.80 Å to the (110) surface or that of 2.05 Å to the {111} micro-facets, which are built by forming a surface vacancy on Al(110) (compare Fig. 7 (e)). The height above the {111} micro-facets is more relevant here than that above the (110) surface because all substrate nearest neighbors of the two adsorbates belong to these {111} micro-facets, and we showed already that the nearest neighbor environment determines the bonding to a large extent as a consequence of the good screening of Al. The adsorption energy can therefore be approximated by $E_{(100)}^{\text{ad}} = 3.77$ eV of an Al adatom on the fourfold site on Al(100), which sits 1.69 Å above the surface (see Table IX in the appendix). This gives an estimated energy barrier of $E_{(110)}^{\text{vac}} + E_{(110)}^{\text{ad}} - 2E_{(100)}^{\text{ad}} = 0.62$ eV, which equals exactly the energy barrier found in the full calculation.

The success of the simple approach used above to assemble the energy for the exchange configurations from the energies of its constituents exemplifies the role of height and local environment for binding on Al surfaces. This also indicates that the nature of the bonding is very similar for equilibrium adsorption sites and in the examined exchange configurations.

G. Comparison of self-diffusion close to the $\langle 110 \rangle/\{111\}$ and to the $\langle 110 \rangle/\{100\}$ step on Al(111)

The above studies showed that the interaction of an Al adatom with the two kinds of close-packed steps on Al(111) is at larger distances attractive and practically identical. Directly at the step however we identified some important differences in adsorption energies and diffusion barriers and mechanisms.

The results given in Table VI show that the adsorption energies at the fivefold coordinated at-step sites is nearly the same, but that there is a small preference (0.03 eV) for the $\langle 110 \rangle/\{100\}$ step. This energy difference is very small; however it might obey a general rule and is therefore interesting to analyze. According to Nelson et al.,²⁵ it can be explained by the different step formation energies (see Table I). Adsorbing, e. g., an Al atom at the {100}-faceted

step creates two $\{111\}$ -faceted “micro-steps” (The situation is reversed at the $\{111\}$ step). The creation of $\{111\}$ -micro-steps should be favorable, because $\{111\}$ -faceted steps are favorable. According to this model, the adsorption energies should differ by 2×0.017 eV. Indeed, the calculated at step adsorption energy difference is very close to this value.

It is tempting to apply the same type of discussion also to the creation of vacancies within the step. To form a vacancy at the $\{100\}$ -faceted step creates $\{111\}$ -micro-steps and should be favorable. However, the full calculations show that such analysis is not appropriate; the vacancy formation energy at the $\{111\}$ -faceted step is energetically favorable (see in Table I).

1. Diffusion along the step

The results of Table VI imply that an Al adatom diffusing along the $\{100\}$ step will use the normal bridge hopping mechanism and not the exchange mechanism as at the (100) surface or at the $\{111\}$ step. The main reason for this difference between the two steps is that the adsorption energy at the long-bridge position at the $\{100\}$ step is 0.19 eV higher. We understand this as an effect of geometry (see, e. g., Figs. 6 and 7(b)). Whereas at the long-bridge position of the $\{111\}$ step the adsorbate is clearly twofold coordinated, the coordination is nearly fourfold at long-bridge position at the $\{100\}$ step. The exchange-parallel configurations at the $\{111\}$ step and at the $\{100\}$ step have practically the same energies. As a consequence it follows that the diffusion at the lower terrace parallel to the $\{100\}$ step proceeds via hopping mechanism with an energy barrier about 0.1 eV lower than that for the exchange diffusion along the $\{111\}$ step. The different diffusion mechanisms should lead to different diffusion prefactors D_0 . The impact of this difference for the temperature dependence of crystal growth is discussed below in Section VI.

2. Diffusion across the step

For diffusion across the $\{111\}$ and the $\{100\}$ step we obtain in both cases exchange diffusion mechanisms with nearly the same energy barrier heights (see Figs. 5 and 6). For the diffusion across the step in the descending direction the energy barriers are very small (0.06 eV and 0.08 eV); in fact they are only marginally larger than that for the diffusion on the flat Al (111) surface.

The exchange path at the $\{100\}$ -faceted step is geometrically quite different from that at the $\{111\}$ -faceted step,⁷³ as it has no mirror symmetry perpendicular to the step. We mapped out a two-dimensional total-energy surface, varying the x - and y -coordinates of the involved step atom (atom 2 in Fig. 6) on a 4×4 grid while relaxing all the other coordinates of the adsorbates and the two upper substrate layers. In addition we calculated the energy for 4 points on the apparent diffusion path. We then checked if all the atomic configurations were smoothly connected along the diffusion path or if some atomic coordinates change drastically between adjacent configurations. The results show that all coordinates vary smoothly, which confirms that the described path is physically relevant.

VI. UNIFORMITY IN SURFACE SELF-DIFFUSION ON METALS: ENERGY BARRIERS AND DIFFUSION MECHANISMS

It is interesting to compare our results for Al surface self-diffusion to those for other fcc metals. The results in Table V show that the rule of thumb which says that diffusion barriers scale with the cohesive energy is valid. We also see, that the energy barriers for surface self-diffusion are clearly lowest for the flattest surface, namely (111) . All rougher surfaces have diffusion barriers about 5 times higher than the (111) surface of the same metal. The diffusion barriers on these rougher surfaces vary by less than a factor of two between different metals.

Important for a description of diffusion and its dependence on the local geometry is the fact that in experiment (and in theory) the barriers for diffusion in the channels of the (110) surface and along the $\{111\}$ -faceted steps of the (331) surface have nearly the same barriers. The only counter example seems to be Ir, but there the barriers for diffusion along the step represent only estimates. We assume that the diffusion mechanism is the exchange (see Fig. 7(d)) in both cases for all metals considered.

In agreement with our results for Al, the experiments show smaller energy barriers for diffusion along the $\{100\}$ step than along the $\{111\}$ step. One might speculate that this difference of the barriers is connected with the change in diffusion mechanism; we remind that for Al we found that the diffusion along the $\{100\}$ step proceeds by a hopping mechanism while it proceeds via exchange along the $\{111\}$ step.

Additional insights about the uniformity of diffusion at fcc (111) surfaces can be obtained from the diffusion prefactors D_0 . Using transition-state theory and semi-empirical calculations, D_0 was evaluated for a series of metal surfaces.^{23,26} In all cases the prefactor of an exchange process was larger than that of the normal hopping diffusion (see also Table VII for Al). Furthermore, we see in Table VII that the experimentally determined diffusion prefactors are larger in the cases where we expect exchange diffusion. Thus, from the larger diffusion prefactors we conclude that for Rh, Pt, and Ir there is hopping diffusion on the (111) surface and along the {100}-faceted step, and exchange diffusion otherwise (see Table VII).

VII. ATOMIC PROCESSES AND GROWTH OF AL (111) AT DIFFERENT TEMPERATURES

The above discussed results for diffusion mechanisms, energy barriers, and diffusion prefactors will now be used for an examination of the temperature dependence of growth of Al(111). The mode of growth is controlled by the interplay of the deposition rate and of the temperature dependent processes of diffusion and defect creation and annihilation. With the information of previous sections at hand we can estimate the most important features of this temperature dependence. An extended study with our results and employing a Monte-Carlo technique^{18,20,21} to evaluate the relevant rate equations, would be certainly superior.

Here we assume that the temperature dependence of the diffusion constant is given by

$$D = D_0 \exp(-E_d/k_B T), \quad (5)$$

where E_d is the energy barrier of the considered diffusion process (see Table IV and VI). The pre-exponential factor D_0 can be estimated from the adatom attempt frequency ν_a and the distance between neighboring adsorption sites, l , as $D_0 = \nu_a l^2/n$. The factor n equals 2 or 4, depending on the dimensionality of the diffusion process. ν_a can be calculated within transition-state theory from the the total-energy surface.^{16,17} On the other hand, D_0 can also be taken from experimental results for similar diffusion processes (see Table VII).

Writing $D_0 = \nu_j l^2/n$ and defining the temperature T_d at which a certain diffusion mechanism becomes active as that at which the adatom will jump at least once per second ($\nu_j = 1/s$), it follows that

$$T_d = \frac{E_d}{k_B} / \ln \frac{nD_0}{\nu_j l^2}. \quad (6)$$

In Table VII we give our choice for D_0 , based on theoretical results for the Al surface diffusion as well as on experimental data for Rh, Pt, and Ir. This choice is clearly not unambiguous; one has to consider, however, that an error of a factor of 10 in D_0 changes the temperature T_d by less than 10 %. The results of the above procedure to determine onset temperatures for diffusion are given in Table VIII.

For temperatures below 320 K the desorption of adatoms from steps is practically irrelevant (see, e.g., Fig. 6 and Table VIII). Thus adatoms captured at a step edge will stay and the island will grow. The processes important for growth at temperatures below 320 K are therefore the capture of Al adatoms at the steps and the diffusion along the steps and their relative rates.

The following approximate analysis of temperature ranges for different growth modes assumes a deposition rate of 1/100 ML/s. The further assumption is that for this deposition rate a jump rate of $\nu_j = 1/s$ is large enough in order for a deposited Al adatom to diffuse to a more stable site before other deposited adatoms meet the first one and form a nucleus. If the deposition rate is higher than 1/100 ML/s then the necessary jump rate to get the same growth mode has to be increased proportionally. This implies that the temperature has to be increased logarithmically (see Eq. 6).

The analysis implies:

- Our calculations show that an Al dimer on Al(111) is bound by 0.58 eV and is therefore stable at temperatures below $\simeq 250$ K. If the mobility of the dimer is smaller than that of the single adatom it will serve as a nucleus for the growth of the next layer. In that case three-dimensional growth would occur whenever two adatoms meet on the upper terrace at a substantial rate.⁶
- At temperatures below 25 K adatoms on the upper terrace are hindered by the step-edge energy barrier to move down (see Table VIII). We note that island edges are frayed at this temperature (see next item), which may reduce the barrier, and adatoms gain energy by adsorption and by approaching the upper step edge, which might lead to some transient mobility.^{13,21} Furthermore we note that on small and/or narrow islands the attempts to overcome the step-edge barrier are more frequent which increases the chance for a success. We are therefore not convinced that the three-dimensional growth mode really exists for clean Al(111).

- For $25 \text{ K} < T < 155 \text{ K}$ the energy barriers of diffusion parallel to both close-packed steps will prevent diffusion parallel to the steps. The diffusion at flat parts of the surface is, however, still easy and therefore the attraction of gas-like adatoms towards the steps edges is still active. As a consequence we expect that islands will be formed in a way which may be described as a “hit-and-stick” mechanism. Thus, the edges cannot equilibrate and fractal-shaped islands with a layer-by-layer growth mode should result.
- For $T > 155 \text{ K}$ the step edges will be straight, as diffusion along the step is possible, and therefore the islands will be triangular or hexagonal. According to a simple model by Michely *et al.*¹⁰ the different diffusion properties for atoms at the two kinds of step edges might become important for determination of the detailed growth form of the island. The model says that the growth perpendicular to the step with the lower adatom mobility will advance fastest. If the growth speed of one step is faster by more than a factor of two than that of the other step the faster one will eventually disappear. As a consequence the growth shape of the island would be triangular. For Al(111) our results imply that at low temperature the diffusion parallel to the {111} step is hindered more than that parallel to the {100} step because of the higher diffusion barrier. However, because the diffusion mechanism is different at these two steps the prefactor for the diffusion parallel to the {100} step is smaller (see Table VII). As a consequence, at higher temperature the diffusion coefficient for the movement parallel to the {100} step will be smaller than that for the movement parallel to the {111} step.⁷⁶

The additional assumption in Ref. 10 is that the growth speed of steps with larger diffusion barriers along the step is higher. This is caused by the less efficient atom transport along the step to corners of the growing island. Atoms moving to the corners contribute to the growth of the adjacent step.

We therefore predict that the adatom islands during growth at lower temperature have shorter {111} edges and at higher temperature they have shorter {100} edges. At a medium temperature the growth shape of islands is hexagonal.

- There are two mechanisms for vacancy formation we considered on the Al(111) surface. The direct creation of vacancies on flat Al(111) is expected to happen with a rate above 1/s per surface-atom at temperatures above 730 K (see Table VIII). In the presence of Al-adatoms the vacancy creation should already take place at 490 K, due to the then reduced barrier (see Table VIII). Adatoms can be provided either from deposition or by desorption from the step. The relatively high energy barriers to create adatoms lets us assume, that the adatom assisted vacancy formation will not be important before the formation of vacancies on the flat Al(111) sets in at 730 K.

The second possibility to create vacancies is at steps. At a {100}-faceted step they will be created with rates of 1/s and step-atom at a temperature of 320 K. At a {111}-faceted step this temperature is 380 K (see Table VIII). These vacancies could migrate into the terrace and become “normal” surface vacancies. The barrier for vacancy migration is 0.56 eV on the flat Al(111), so it becomes active at 240 K (see Tables V and VIII). The onset temperature for vacancy generation from steps therefore should be 320 K. Vacancy generation and diffusion into the terrace was also observed in STM experiments on Pt(111),³² which again shows the similarity of atomic processes on Pt(111) and Al(111).

VIII. CONCLUSION

In conclusion, we have presented results of accurate electronic structure and total-energy calculations which reveal several phenomena directly relevant to the description of self-diffusion at Al surfaces and to crystal growth.

The three low index surfaces of Al are quite different with regard to surface self diffusion. The diffusion barriers for Al adatoms on Al(111) [$E_d = 0.04 \text{ eV}$] are much lower than on Al(100) and Al(110) [$E_d = 0.33 - 0.62 \text{ eV}$]. For Al(100) and Al(110) atomic exchange mechanisms have lower barriers for surface self diffusion than ordinary hopping. Exchange diffusion was found even in the direction parallel to the atomic rows on Al(110). The diffusion of surface vacancies was studied for the Al(111) surface ($E_d = 0.56 \text{ eV}$).

Our calculations predict that Al adatoms on Al(111) are attracted towards the edge of close packed steps by a long-range force which most likely originates from a interaction of adatom and step induced surface states. Adatoms close to the lower step edge are funneled towards the step. The diffusion of an Al adatom from the upper to the lower terrace proceeds via an exchange of the on-terrace adatom with an in-step-edge substrate atom. The barrier for this exchange process is rather low which leads to layer-by-layer growth down to very low temperatures. Corresponding results have been observed in field-ion microscopy studies of W and Ir adatoms on Ir(111) by Wang and Ehrlich.^{34,55}

On Al(111) the energy barrier for diffusion of an Al at-step adatom parallel to the step is much bigger than that perpendicular to the step in the descending direction. In the temperature range where this energy barrier becomes

relevant, we expect fractal growth. The mechanism for diffusion along the two kinds of steps is different. Along the $\{111\}$ -faceted steps we find an atomic replacement mechanism similar to that for diffusion parallel to the rows on Al(110), along the $\{100\}$ -faceted steps the hopping mechanism has the lowest energy barrier. The differences in energy barrier and diffusion prefactor for diffusion along the two kinds of steps can lead to temperature dependent growth forms of islands. Surface systems where similar growth phenomena were observed experimentally are Pt on Pt(111)^{9,10} and Au on Ru(0001).¹¹

A comparison of our results for self diffusion on Al surfaces and of other theoretical and experimental results on transition metals indicate that atomic exchange processes in surface self diffusion are more common than assumed previously.

We predict that $\{111\}$ -faceted steps on Al(111) are energetically favorable compared to the $\{100\}$ -faceted steps. A similar energy difference was found for Pt(111) in experiment.⁹

Additionally to the energetics at Al surfaces we have discussed the surface dipole moments induced by adatoms and steps on the Al(111) surface and, related to that, the work function differences of the low index surfaces of Al. Our results indicate that the commonly used model based on Smoluchowski smoothing alone²⁸ has to be modified.

APPENDIX A: AL ON AL (100)

We add here our results for the adsorption and diffusion of Al on Al(100). Our study repeats that of Feibelman on the same system.⁷⁴ The main result of Feibelman's paper, which is the favorable energy barrier for an exchange diffusion mechanism, has been questioned recently.^{23,75} We calculated the adsorption energies at the three sites which are important for the discussion of surface diffusion (see Fig. 8). Our results confirm that the exchange diffusion mechanism has a lower barrier than the bridge diffusion mechanism. The agreement in adsorption energy differences of our results with those of Feibelman is again as excellent as in the other examples in this paper. However, this agreement with Feibelman's results is obtained only, if we use the same slab thickness as he did, i.e., 5-layers (see Table IX). The agreement would be even better, if we had not relaxed all atoms but only those which Feibelman had relaxed. However, while the numerical accuracy of both calculations agree, it is most interesting to note that our calculations with 6 and 7 layer slabs show a significant change of the energy of the exchange configuration. This change increases the barrier for diffusion by nearly a factor of three (see Table IX). A similar sensitivity of calculated energies with slab thickness was not found for any other system and we do not have an explanation for it. The energy of the exchange configuration also proved to be especially sensitive to changes in the value of the lattice constant and the \mathbf{k} -point sampling.

* present address: Sandia National Laboratories, Division 1114, Albuquerque, NM 87185-0344

¹ G. Ayrault and G. Ehrlich, *J. Chem. Phys.* **60**, 281 (1974).

² S. C. Wang and G. Ehrlich, *Phys. Rev. Lett.* **62**, 2297 (1989).

³ G. L. Kellogg, *Surf. Sci.* **246**, 31 (1991).

⁴ T. T. Tsong and C.-L. Chen, *Phys. Rev. B* **43**, 2007 (1991).

⁵ T. T. Tsong, *Atom-probe field ion microscopy*, Cambridge University Press (1990).

⁶ H. Bethge, p. 125 in *Kinetics of Ordering and Growth at Surfaces*, ed. by M. Lagally, Plenum Press (New York, 1990).

⁷ M. Klaua, H. Bethge, *Ultramicroscopy* **17**, 73 (1985).

⁸ R. Kunkel, B. Poelsema, L.K. Verheij, and G. Comsa, *Phys. Rev. Lett.* **65**, 733 (1990).

⁹ M. Bott, T. Michely, and G. Comsa, *Surf. Sci.* **272**, 161 (1992).

¹⁰ T. Michely, M. Hohage, M. Bott, and G. Comsa, *Phys. Rev. Lett.* **70**, 3943 (1993).

¹¹ R.Q. Hwang et al., *Phys. Rev. Lett.* **67**, 3279 (1991).

¹² S. C. Wang and G. Ehrlich, *Surf. Sci.* **239**, 301 (1990).

¹³ W. F. Egelhoff Jr. and I. Jacob, *Phys. Rev. Lett.* **62**, 921 (1989).

¹⁴ B. J. Hinch, R. B. Doak, and L. H. Dubois, *Surf. Sci.* **286**, 261 (1993).

¹⁵ S. Oppo, V. Fiorentini, and M. Scheffler, *Phys. Rev. Lett.* **71**, 2437 (1993).

¹⁶ G. Vineyard, *J. Phys. Chem. Solids* **3**, 121 (1957).

¹⁷ R. Gomer, *Rep. Prog. Phys.* **53** 917-1002 (1990).

¹⁸ J. A. Venables, G. D. T. Spiller, and M. Hanbücken, *Rep. Prog. Phys.* **47** (1984).

¹⁹ J. Villain, *J. Phys. I* **1** 19 (1991); Z.-W. Lai and S. Das Sarma, *Phys. Rev. Lett.* **66**, 2348 (1991); Hong Yan, *Phys. Rev. Lett.* **68**, 3048 (1992).

²⁰ S. Kenny, M. R. Wilby, A. K. Myers-Beaghton, and D. D. Vvedensky, *Phys. Rev. B* **46**, 10345 (1992).

²¹ P. Šmilauer, M. R. Wilby, and D. D. Vvedensky, *Phys. Rev. B* **47**, 4119 (1993).

²² K.D. Hammonds and R.M. Lynden-Bell, *Surf. Sci.* **278**, 437 (1992).

²³ C. L. Liu, J. M. Cohen, J. B. Adams, and A. F. Voter, *Surf. Sci.* **253**, 334 (1991).

²⁴ C.-L. Liu and J.B. Adams, *Surf. Sci.* **265**, 262 (1992).

²⁵ R. C. Nelson, T. L. Einstein, S. V. Khare, and P. J. Rous, *Surf. Sci.* **295**, 462 (1993).

²⁶ L. B. Hansen, P. Stoltze, K. W. Jacobsen, and J. K. Nørskov, *Phys. Rev. B* **44**, 6523 (1991); L. B. Hansen, P. Stoltze, K. W. Jacobsen, and J. K. Nørskov, *Surf. Sci.* **289**, 68 (1993).

²⁷ R. Smoluchowski, *Phys. Rev.* **60**, 661 (1941).

²⁸ A. Zangwill, *Physics at Surfaces*, University Press, Cambridge (1988).

²⁹ W. E. Pickett, *Comp. Phys. Rep.* **9**, 117 (1989).

³⁰ Some of the calculations presented here were reported previously in M. Scheffler, J. Neugebauer, and R. Stumpf, *J. Phys.: Cond. Matter* **5**, A91 (1993), in R. Stumpf and M. Scheffler, *Phys. Rev. Lett.* **72**, 254 (1994), and in R. Stumpf and M. Scheffler, *Surf. Sci.* **307-309**, 501 (1994).

³¹ B. Lang, R. W. Joyner, and G. A. Somorjai, *Surf. Sci.* **30**, 440 (1972); M. A. van Hove and G. A. Somorjai, *Surf. Sci.* **92**, 489 (1980); D. R. Eisner and T. L. Einstein, *Surf. Sci.* **286**, L559 (1993).

³² T. Michely and G. Comsa, *Surf. Sci.* **256**, 217 (1991); T. Michely, T. Land, U. Littmark, and G. Comsa, *Surf. Sci.* **272**, 204 (1992).

³³ C.-L. Chen and T. T. Tsong, *Phys. Rev. B* **47**, 15852 (1993).

³⁴ S.C. Wang and G. Ehrlich, *Phys. Rev. Lett.* **67**, 2509 (1991).

³⁵ K. Besocke, B. Krahl-Urban, and H. Wagner, *Surf. Sci.* **68**, 39 (1977).

³⁶ R. Stumpf and M. Scheffler, *Computer Physics Communications*, **79**, 447, Cat. No. ACTF (1994).

³⁷ D. M. Ceperley and B. J. Alder, *Phys. Rev. Lett.* **45** (1980) as parameterized by J. P. Perdew and A. Zunger, *Phys. Rev. B* **23**, 5048 (1981).

³⁸ W. Kohn and L. J. Sham, *Phys. Rev.* **140**, A1133 (1965).

³⁹ R. Car and M. Parrinello, *Phys. Rev. Lett.* **55**, 2471 (1985).

⁴⁰ A. Williams and J. Soler, *Bull. Am. Phys. Soc.* **32**, 562 (1987).

⁴¹ R. Stumpf, X. Gonze, and M. Scheffler, Research report of the Fritz-Haber-Institut, April (1990), and X. Gonze, R. Stumpf, and M. Scheffler, *Phys. Rev. B* **44** 8503 (1991).

⁴² H. J. Monkhorst and J. D. Pack, *Phys. Rev. B* **13**, 5188 (1976).

⁴³ M. J. Gillan, *J. Phys. Cond. Matt.* **1**, 689 (1989).

⁴⁴ J. Neugebauer and M. Scheffler, *Phys. Rev. B* **46**, 16067 (1992).

⁴⁵ A. de Vita and M. J. Gillan, *J. Phys. C: Cond. Matt.* **3**, 6225 (1991).

⁴⁶ G. Kresse, J. Haffner, *Phys. Rev. B* **48**, 13115 (1993).

⁴⁷ C. Kittel, *Introduction into Solid State Physics*, 6th Edition, Wiley (1986).

⁴⁸ There exists a more elegant way to smear the occupation numbers around the Fermi energy introduced in M. Methfessel and A. T. Paxton, *Phys. Rev. B* **40**, 3616 (1989). There the total energy is minimized so that the energies and forces do not have to be corrected. We therefore used this method in later studies.

⁴⁹ M. R. Pederson and K. A. Jackson, *Phys. Rev. B* **43**, 7312 (1991).

⁵⁰ K.-M. Ho, J. Ihm, and J. D. Joannopoulos, *Phys. Rev. B* **25**, 4260 (1982), and T. A. Arias, M. C. Payne, and J. D. Joannopoulos, *Phys. Rev. B* **45**, 1538 (1992).

⁵¹ M. W. Finnis, *J. Phys.: Cond. Matt.* **2**, 331 (1990).

⁵² The gain in speed by using more sophisticated update techniques like the conjugate gradient approach⁴³ would be small for large metallic systems, according to our experience.

⁵³ J. S. Nelson and P. J. Feibelman, *Phys. Rev. Lett.* **68**, 2188 (1992).

⁵⁴ P. J. Feibelman, *Phys. Rev. Lett.* **69**, 1568 (1992). The adsorption energies given in this paper are not directly comparable to ours (see Ref. 56) because of the reference energy of the isolated atom. Apparently there is an inconsistency of this reference energy caused by Feibelman's Greens-function technique; energy differences are comparable, however, and for these the main (but small) differences to our results arise because Feibelman did not include the adsorbate-induced relaxation of the Al(331) substrate.

⁵⁵ S.C. Wang and G. Ehrlich, *Phys. Rev. Lett.* **70**, 41 (1993).

⁵⁶ Cohesive and adsorption energies are given with respect to the energy of an isolated Al atom calculated in a large cell with the same 8 Ry cut-off. Adding the spin-polarization energy of 0.15 eV gives the cohesive energy as 4.15 eV which is 0.75 eV higher than the experimental value. This overbinding is a problem common to converged DFT-LDA calculations. It is widely accepted that adsorption energy differences for different sites are practically unaffected by this problem. An Al atom adsorbed at a kink site gains exactly the cohesive energy.

⁵⁷ The embedding charge density is the central quantity in embedded atom and effective medium theory.^{58,59} The embedding

density is closely connected to the coordination number of the adsorbate, so that coordination and embedding may in fact be regarded as different names for the same thing.

⁵⁸ M. S. Daw and M. I. Baskes, Phys. Rev. B, **29**, 12 (1984).

⁵⁹ K. W. Jacobsen, J. K. Nørskov, and M. J. Puska, Phys. Rev. B **35**, 7423 (1987).

⁶⁰ "Simple bond-cutting" models assume that the energy per atom varies linearly with the atom's coordination number. An improved version which takes the bond saturation into account makes this approach very similar to the effective-medium and embedded-atom methods (see for example I.J. Robertson et al., Europhys. Lett. **15**, 301 (1991), Phys. Rev. Lett. **70**, 1944 (1993), and M. Methfessel et al., Appl. Phys. A **55**, 442 (1992)).

⁶¹ A dipole moment of 1 debye equals $2.4e/\text{\AA}$ were e is the electronic charge.

⁶² J. K. Grepstad, P. O. Gartland, and B. J. Slasvold, Surf. Sci. **57**, 348 (1976).

⁶³ The values for the work functions were determined by averaging values for slabs of thickness 5 to 7 layers for Al(111) and 8 and 9 layers for Al(110).

⁶⁴ J. Hölzl and F.K. Schulte, in *Springer Tracts in Modern Physics* **85**, p. 1-100, Springer, Berlin (1979).

⁶⁵ H. Ishida and A. Liebsch, Phys. Rev. B **46**, 7153 (1992).

⁶⁶ A. P. Seitsonen and M. Scheffler, in preparation.

⁶⁷ C. Stampfl, M. Scheffler, H. Over, J. Burchhardt, M. Nielsen, D. L. Adams, and W. Moritz, Phys. Rev. B, accepted; Phys. Rev. Lett.

⁶⁸ B. Hammer, K. W. Jacobsen, V. Milman, and M. C. Payne, J. Phys.: Cond. Matt. **4**, 10453 (1992).

⁶⁹ R. T. Tung and W. R. Graham, Surf. Sci. **97**, 73 (1980).

⁷⁰ D.W. Basset and P.R. Webber, Surf. Sci. **70**, 520 (1978).

⁷¹ M. F. Crommie, C. P. Lutz, and D. Eigler, Nature **363**, 524 (1993).

⁷² Y. Hasegawa and P. Avouris, to be published (1993).

⁷³ There could be a nonsymmetric exchange path at the {111}-faceted step also. We did not calculate that path as the symmetric one has already such a low barrier which is at the limit of the accuracy of our calculations. Our conclusions therefore would not be affected by an additional diffusion process. No energetically favorable symmetrical exchange path exists for the {100}-faceted step, as there the involved step atom would have to go over a top site.

⁷⁴ P. J. Feibelman, Phys. Rev. Lett. **65**, 729 (1990).

⁷⁵ S. Debiaggi and A. Caro, J. Phys.: Cond. Matt. **4**, 3905 (1992).

⁷⁶ We can estimate the temperature T^{cross} at which diffusion along the two kinds of steps will proceed at the same rate. Transforming Eq. 5 to

$$T^{\text{cross}} = k \frac{E_d^{\{111\} \parallel} - E_d^{\{110\} \parallel}}{\ln D_0^{\{100\} \parallel} - \ln D_0^{\{111\} \parallel}}$$

and taking the values for D_0 and E_d for the {110}/{111}- and {110}/{100} step from Tables VII and VIII, we get $T^{\text{cross}} \simeq 400$ K. We expect that this value is rather inaccurate however.

TABLE I. Surface, step, adatom, and vacancy formation energies for aluminum. The Al chemical potential is taken as the cohesive energy, i.e. 4.15 eV.⁵⁶ Thus, the adatom is considered to be taken from a bulk or kink site, and for the vacancy formation energies the removed atom is put into such site.

system	surface and step formation (eV/atom)	(eV/Å ²)	adatom formation (eV)	vacancy formation (eV)
Al(111)	0.48	0.070	1.05	0.67
Al(100)	0.56	0.071	0.38	0.65
Al(110)	0.89	0.080	0.26	0.12
$\langle 110 \rangle / \{111\}$ -step	0.232	0.082	0.28	0.21
$\langle 110 \rangle / \{100\}$ -step	0.248	0.088	0.25	0.24

TABLE II. Total-energy difference ΔE per edge atom of two triangular islands on a 4-layer thick Al(111) slab in eV. One island has only {111}- and the other one has only {100}-faceted steps. Four different island sizes are considered. Using a 5-layer substrate changes the results by < 10 %. The data in the rightmost column were obtained with the atoms of the islands relaxed. Relaxing more atoms does not change the energy differences significantly.

# atoms	# edge atoms	surf. cell	$\Delta E^{\text{unrelaxed}}$	$\Delta E^{\text{relaxed}}$
6	6	6 × 5	0.025	0.029
10	9	6 × 5	0.019	0.021
15	12	6 × 6	0.017	0.018
21	15	8 × 7	0.017	0.018

TABLE III. Induced dipole moment μ of Al adsorbates on fcc and hcp sites of Al(111) at 1/16 ML coverage and of a step atom in {111}- and {100}-faceted steps on Al(111) in debye.⁶¹ Positive μ means that the negative end of the dipole points into the vacuum. Results are given for the substrate atoms unrelaxed and relaxed. The numerical accuracy of the given values is ± 0.01 debye. The values are averages for slabs of 5 to 7 layers thickness.

system	$\mu^{\text{unrelaxed}}$	μ^{relaxed}
fcc-site adatom	0.13	0.30
hcp-site adatom	0.06	0.24
{111}-faceted step	-0.01	-0.01
{100}-faceted step	0.045	0.045

TABLE IV. Total energies for an isolated Al adatom on Al(111) at fcc, bridge, hcp, and top sites and on the fcc or hcp site directly at the upper side of the {111}- and the {100}-faceted step. The energy zero is the energy of a free aluminum atom.⁵⁶ For the adsorption on the flat Al(111) surface also the adsorbate height is given with respect to the center of the top substrate layer.

site	coordination	E (eV)	h (Å)
fcc	3	-3.06	2.11
bridge	2	-3.06	2.09
hcp	3	-3.10	2.08
top	1	-2.57	2.12
fcc on $\langle 110 \rangle / \{111\}$ -step	3	-3.18	—
hcp on $\langle 110 \rangle / \{100\}$ -step	3	-3.18	—

TABLE V. Comparison of calculated energy barriers (in eV) for surface self-diffusion on Al with those by embedded-atom calculations of Liu et al.⁵⁸ for Al (two potentials were used there; both results deviate considerably from ours) and with experimentally determined barriers on other metal surfaces. The experimental results were determined using field ion microscopy. Values in brackets are believed to be less accurate, as they were obtained with an assumed value for the diffusion prefactor D_0 . The symbols \parallel and \perp indicate a diffusion direction parallel or perpendicular to the channels of the (110) surface or to the step edge respectively.

surface	Al (this work)	Al ²³		Ni ^{23,69}	Rh ¹	Pt ^{3,70}	Ir ^{2,4,5,12}
(111) vacancy at Al(111)	0.04	0.054	0.074	—	0.16	(0.12)	0.27
	0.56	—	—	—	—	—	—
(100)	0.35	0.69	0.25	—	0.63	0.47	0.84
(110) \parallel	0.33	0.26	—	(0.45)	0.60	0.84	0.80
(110) \perp	0.62	0.30	0.15	(0.45)	—	0.78	0.71
$\langle 110 \rangle / \{111\}$ -step \parallel or $(332)\parallel$	0.42	0.27	0.24	(0.45)	0.64	0.84	(1.05)
$\langle 110 \rangle / \{100\}$ -step \parallel or $(644)\parallel$	0.32	0.20	0.24	(0.37)	0.54	0.69	(0.96)
cohesive energy ⁴⁷		3.39		4.44	5.75	5.84	6.94

TABLE VI. Total energies E for Al adatoms with respect to that of a free Al atom and energy barriers ΔE (both in eV) for sites with similar local geometry on the Al(110), the Al(331) surface and at steps on Al(111) (compare Fig. 7).⁵⁶ The results for the (331) surface may be compared to those for the $\langle 110 \rangle / \{111\}$ step. For the adsorption on Al(110) we give also the height h (in Å) above the relaxed, flat surface. As explained in the text, the exact barriers for exchange diffusion parallel to the step edge might be 0.04 eV higher than given in the table.

	Al(110)		Al(331) ^a	$\langle 110 \rangle / \{111\}$ -step		$\langle 110 \rangle / \{100\}$ -step
	E	h	E	E	E	E
(a) fivefold site	-3.89	1.33	-3.68	-3.87		-3.90
diffusion	ΔE		ΔE	ΔE	ΔE	ΔE
(b) long bridge	-0.60	1.58	-0.57	-0.48		-0.32
(c) short bridge	-1.06	2.16	-1.21	-1.03		-1.15
(d) exchange \parallel	-0.33	1.27	—	-0.39		-0.44
(e) exchange \perp	-0.62	0.80	—	-0.76 (-0.06) ^b		-0.80

^aCalculations by Feibelman;⁵⁴ for technical differences from our calculations see text and reference 54

^bIn brackets we give the barrier for the descending diffusion

TABLE VII. Diffusion prefactors D_0 (in cm^2/s) from theory for Al (mean of the two values given in Ref. 23) and from experiment for Rh, Pt, and Ir surfaces. Values in brackets are considered to be less reliable. The (331) surface has $\{111\}$ -faceted steps and the (311) surface has $\{100\}$ -faceted steps. The column “mechanism” contains our assumptions about the mechanism of diffusion for every row, and the right column gives the diffusion prefactors which will be used in the temperature dependence of growth of Al(111).

surface	mechanism	Al ²³		Rh ¹	Pt ^{3,70}	Ir ^{2,4,5,12}	our choice
(111)	hopping	9×10^{-4}	1.6×10^{-3}	2×10^{-4}	(3×10^{-4})	9×10^{-5}	2×10^{-4}
(100)	exchange	—	4×10^{-2}	(1×10^{-3})	1.3×10^{-3}	6×10^{-2}	8×10^{-3}
(110) \parallel	exchange	—	—	3×10^{-1}	8×10^{-3}	6×10^{-2}	1×10^{-2}
(110) \perp	exchange	6×10^{-2}	2.4×10^{-2}	—	1×10^{-3}	4×10^{-3}	2×10^{-3}
(331) \parallel	exchange	—	—	1×10^{-2}	4×10^{-4}	—	1×10^{-2}
(311) \parallel	hopping	2×10^{-3}	6.7×10^{-3}	2×10^{-3}	(1×10^{-6})	—	5×10^{-4}

TABLE VIII. Energy barriers E_d (in eV) for different self-diffusion and vacancy-formation processes on Al surfaces. From these barriers and from estimates of the pre-exponential D_0 in Eq. 5 (see Table VII) we calculate the temperatures T_d at which these processes happen at a rate of $1/s$ per atom (see Eq. 6). Exchange processes are indicated. Note that the thermodynamical vacancy formation energies as given in Table I are lower than the vacancy formation barriers.

<i>adatom diffusion</i>		E_d (eV)	T_d (K)
flat Al(111)		0.04	17 ± 10
flat Al(100)	[exch.]	0.35	135 ± 23
Al(110) \parallel to rows	[exch.]	0.33	130 ± 23
(110) \perp to rows	[exch.]	0.62	245 ± 34
$\langle 110 \rangle / \langle 111 \rangle$ step \parallel	[exch.]	0.42	155 ± 25
$\langle 110 \rangle / \langle 100 \rangle$ step \parallel		0.32	135 ± 23
$\langle 110 \rangle / \langle 111 \rangle$ step \perp descending	[exch.]	0.06	25 ± 12
$\langle 110 \rangle / \langle 100 \rangle$ step \perp descending	[exch.]	0.08	33 ± 13
<i>other processes on Al(111)</i>			
vacancy diffusion on Al(111)		0.56	240 ± 35
adatom desorption from step		$\simeq 0.8$	$\simeq 320$
vacancy-formation in $\langle 110 \rangle / \{100\}$ step ^a		$\simeq 0.8$	$\simeq 320$
vacancy-formation in $\langle 110 \rangle / \{111\}$ step ^a		$\simeq 0.95$	$\simeq 380$
vacancy-formation on flat surface ^b		1.2 – 1.8	490 – 730

^aEstimated energy barriers, assuming that the transition state is similar to that for bridge diffusion along the step (see Table VI).

^bThe assumed transition state for the higher of the two values is that for bridge diffusion across the step (see Table VI). The lower value corresponds to vacancy-formation in the presence of another Al adsorbate.

TABLE IX. Adsorption energies (in eV) and heights (in bohr) for Al adsorbed on Al(100) at 1/16 ML coverage. The energy zero is the energy of an isolated, free Al atom. The considered configurations are pictured in Fig. 8. Results for slabs of different thickness are compared with those obtained by Feibelman⁷⁴ who used a 5-layer slab. He used the experimental lattice constant of 7.66 bohr and allowed only the adsorbate and its substrate neighbors to relax (see also Ref. 54). On the other hand, we use the theoretical lattice constant of 7.56 bohr, one special \mathbf{k} -point in the surface Brillouin zone, and we allow the adsorbate and the upper two layers to relax. For the results labeled as “average” additional calculations with 4 \mathbf{k} -points and with an additional layer relaxed were considered as well. Energies are in eV, the adsorbate heights h are in Å relative to the relaxed clean surface.

	configuration	E	$\Delta E^{4\text{-fold}}$	h
5-layer (Ref. 74)	4-fold	–2.93	—	1.72
	bridge	–2.28	0.65	2.20
	exchange	–2.73	0.20	0.90
5-layer	4-fold	–3.68	—	1.58
	bridge	–3.05	0.63	1.91
	exchange	–3.55	0.13	0.74
6-layer	4-fold	–3.75	—	1.70
	bridge	–3.12	0.63	2.11
	exchange	–3.37	0.38	0.91
7-layer	4-fold	–3.75	—	1.73
	bridge	–3.07	0.69	2.12
	exchange	–3.35	0.40	0.98
“average”	4-fold	–3.77	—	1.69
	bridge	–3.12	0.68	2.09
	exchange	–3.42	0.35	0.90

FIG. 1. Side view (upper panel) and top view (lower panel) of an orthorhombic supercell, containing a four-atom wide terrace stripe, oriented in $\langle 110 \rangle$ direction, on an Al(111) substrate. Note the different step types at the left terrace edge (a $\{100\}$ micro-facet) and right terrace edge (a $\{111\}$ micro-facet). The two step types are labeled as $\langle 110 \rangle/\{100\}$ and $\langle 110 \rangle/\{111\}$. The three sites important for diffusion on flat Al(111) are also indicated.

FIG. 2. Top and side view of the fcc(332) surface. The (332) surface has $\{111\}$ -faceted steps and the number of atomic rows within the (111) oriented terraces is six.

FIG. 3. Top and side view of the fcc(433) surface. The (433) surface has $\{100\}$ -faceted steps and the number of atomic rows within the (111) oriented terraces is seven.

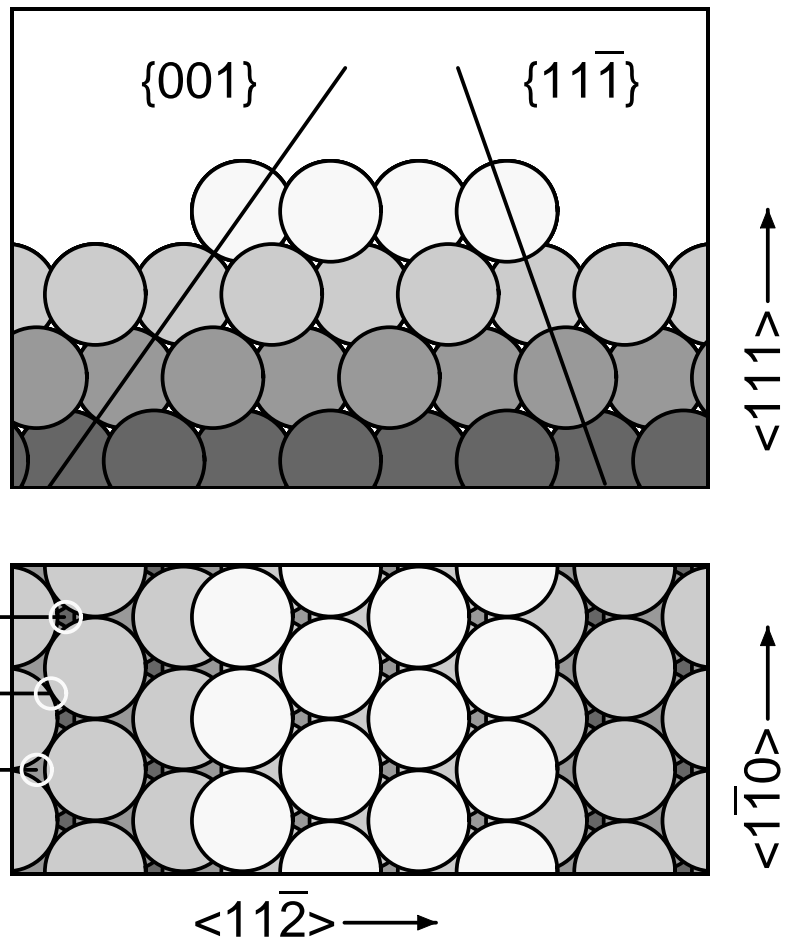
FIG. 4. View at islands on a fcc(111) surface. The two differently oriented triangular islands have only one kind of step; the hexagonal island has both sorts of step.

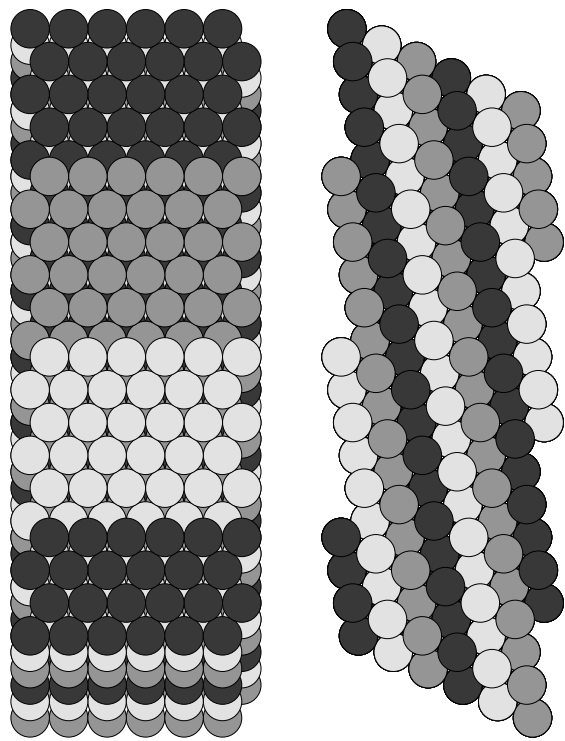
FIG. 5. Total energy along the diffusion path of an Al adatom crossing a $\{111\}$ -faceted step on Al(332) (see also Fig. 2). The upper curve is calculated for the “normal” hopping diffusion and the lower one for the exchange process. The generalized coordinate is $Q = X_1 + X_2$ where X_1 and X_2 are the x -coordinates of the adatom labeled as No. 1 in the atomic-structure plot and X_2 is the position of a step-edge atom labeled as No. 2. The x -axis is parallel to the surface and perpendicular to the step orientation. For the undistorted step $X_2 = 0$. All other coordinates of the diffusing atom and of the two top substrate layers are optimized for each position Q .

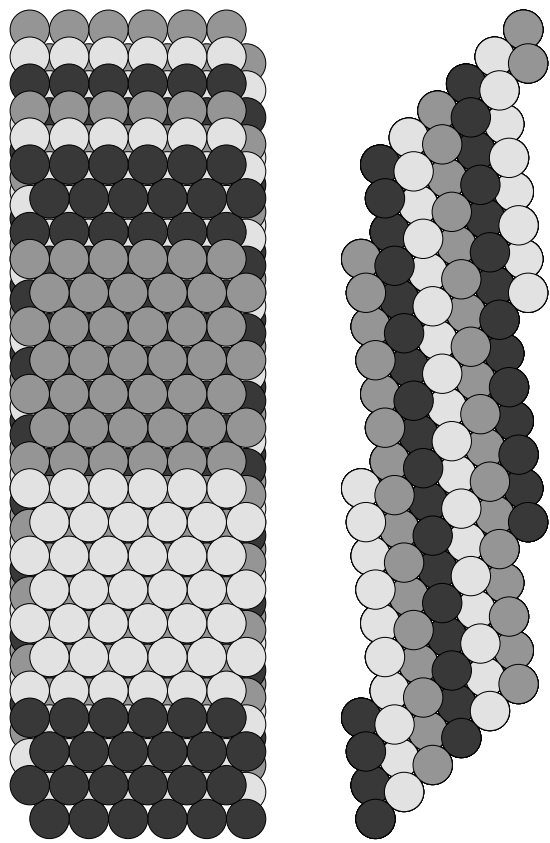
FIG. 6. Upper panel: total energy along the diffusion path on an Al(433) surface for the generalized coordinate $Q = X_1 + X_2$ belonging to the two atoms labeled 1 and 2, which are involved in the exchange process for the across step diffusion (see also Fig. 5). Medium panel: Top view of the Al adatom situated on top of the $\{100\}$ -faceted step. The rectangle gives the range of x - y -coordinates at which atom 2 was set for finding the lowest-energy path (see also Fig. 3). Lower panel: Contour plot of the total energy of the system with the x - y coordinate of atom No. 2 fixed at positions in a regular 4×4 mesh in the rectangle in the medium panel (contour spacing 0.04 eV). All other coordinates of the adsorbates and the two top layers were relaxed. The dashed line connects equivalent points in the two figures, the dashed quarter circles indicate the in-step and the at-step position of atom No. 2.

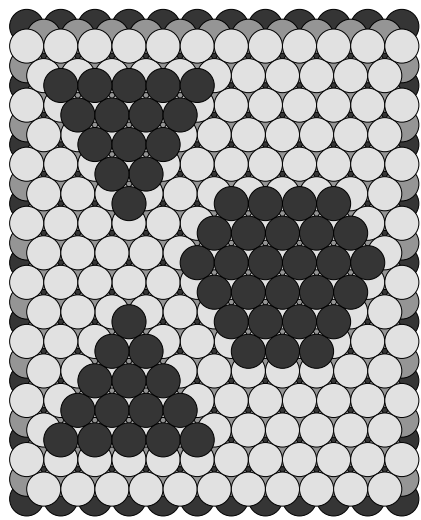
FIG. 7. Important adatom geometries on the (110) surface (top) and at the $\{111\}$ -faceted step on a fcc(111) surface (bottom). The energies of these geometries are given in Table VI.

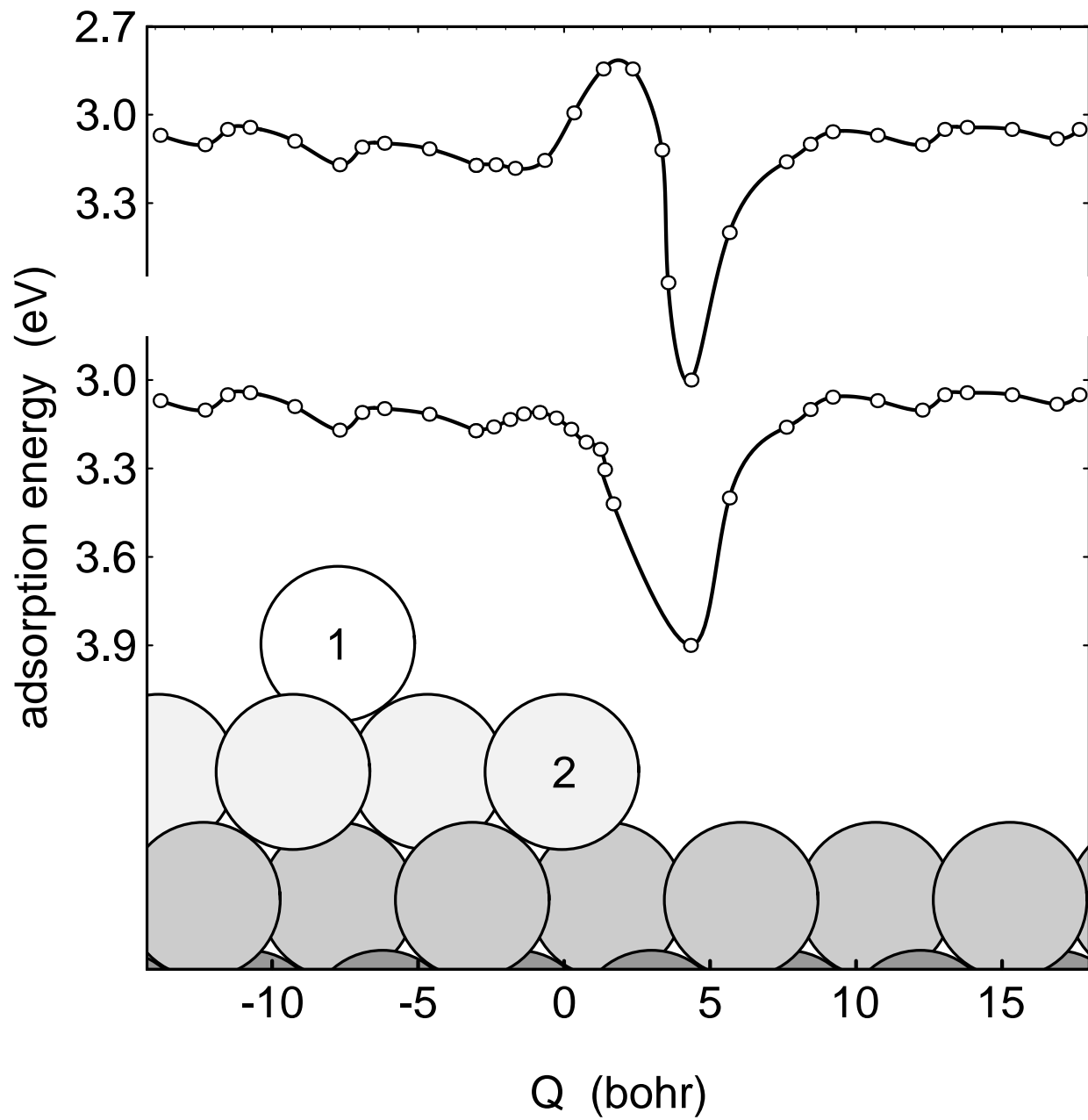
FIG. 8. View at the 3 adsorption geometries considered for the Al self-diffusion on Al(100).

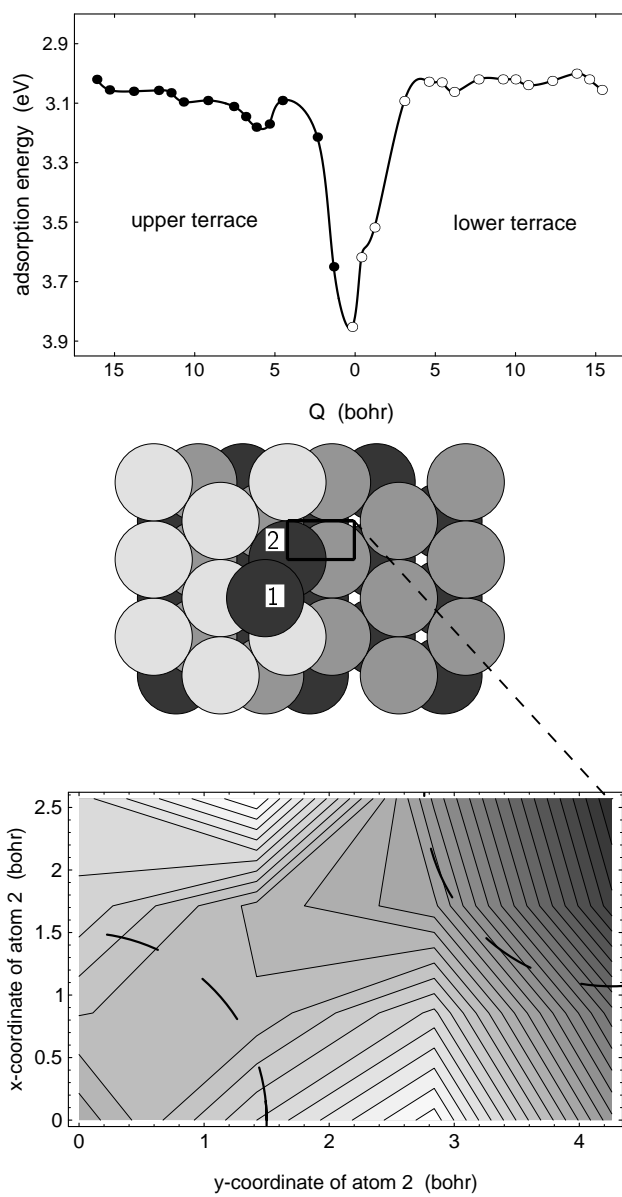


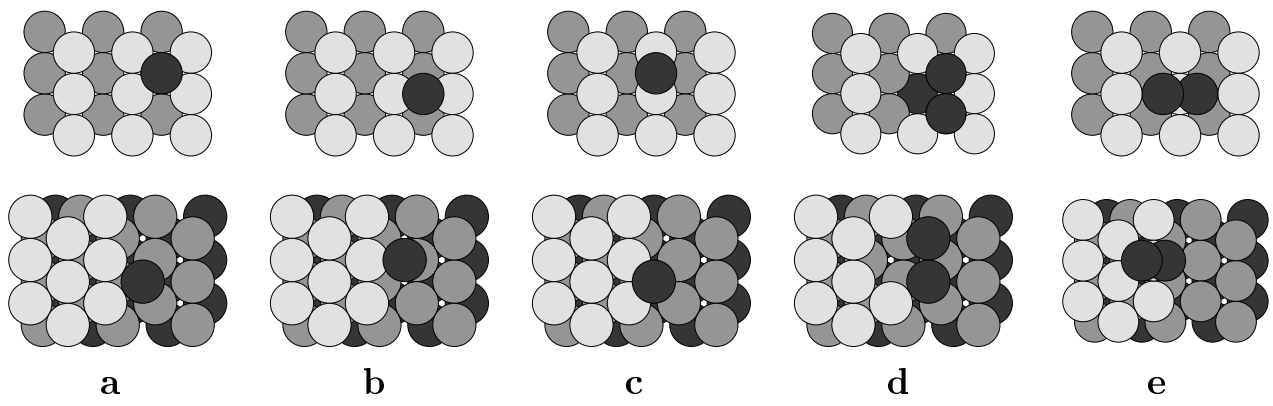


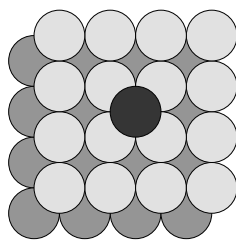




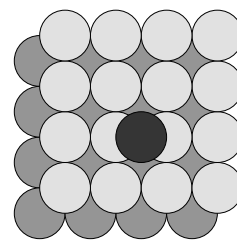




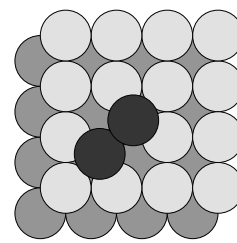




4-fold



bridge



exchange